J|A|C|S
ARTICLES
Published on Web 09/21/2004

Variational Transition State Theory as a Tool To Determine Kinetic Selectivity in Reactions Involving a Valley-Ridge Inflection Point

Àngels González-Lafont, Miquel Moreno, and José M. Lluch*

Contribution from the Departament de Química, Universitat Autònoma de Barcelona, 08193 Bellaterra (Barcelona), Spain

Received November 12, 2003; E-mail: lluch@klingon.uab.es

Abstract: Variational transition state theory has been used to calculate the kinetic isotope effects affecting product ratios in the reaction between $^1O_2$ and d_6-tetramethylethylene. The minimum energy path on the potential energy surface for this process reaches a valley-ridge inflection point and then bifurcates leading to the two final products. Using canonical variational transition state theory, two distinct dynamical bottlenecks were located corresponding to the H- and the D-abstraction, respectively. The calculated KIE at 263 K turns out to be 1.126. Analogously, a H/T KIE of 1.17 at the same temperature has been found for the reaction of $^1O_2$ with the tritiated derivative of tetramethylethylene.

Introduction

Transition-state theory and, in particular, its generalization, variational transition state theory (VTST)[1] have proved to be accurate practical methods for calculating thermal reaction rate constants.[2] The essence of this theory is that it is based on the local dynamics at the dynamical bottleneck. In its canonical version, VTST places that bottleneck at the dividing surface between reactants and products which maximizes the generalized activation free energy. Recently, several authors[3−6] have claimed that transition-state theory is unable to interpret the experimental kinetic selectivity in product formation when the minimum-energy path (MEP) contains a valley-ridge inflection point (VRI)[7−19] after the rate-limiting transition state of the global reaction (that is, in the energy descending region of the potential energy surface (PES) from the rate -limiting transition state to the different products). Their argument was very clear. If there is neither enthalpic nor entropic barriers along the alternative branching pathways that lead to the different products, transition-state theory simply does not apply. Then, the branching ratio of the products must be decided by dynamic effects, outside of the realm of transition-state theory.

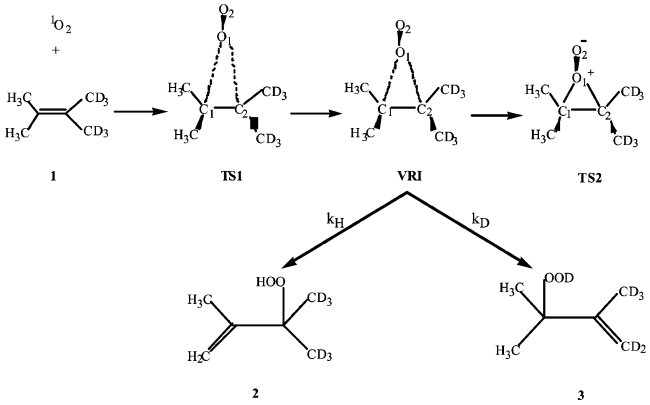

A specially challenging, subtle chemical problem in that field is the H/D kinetic isotope effect (KIE) on the ene reaction of

(1) (a) Truhlar, D. G.; Isaacson, A. D.; Garrett, B. C. *Generalized Transition State Theory* in *Theory of Chemical Reaction Dynamics*; Baer, M., Ed.; CRC Press: Boca Raton, FL, 1985; Vol. 4, pp 65−137. (b) Tucker, S. C.; Truhlar, D. G. *Dynamical Formulation of Transition State Theory: Variational Transition States and Semiclassical Tunneling* in *New Theoretical Concepts for Understanding Organic Reactions*; Bertrán, J., Csizmadia, I. G., Eds.; NATO ASI Ser. C 267; Kluwer: Dordrecht, The Netherlands, 1989; pp 291−346. (c) Garrett, B. C.; Truhlar, D. G. *Transition State Theory* in *Encyclopedia of Computational Chemistry*; Schleyer, P. v. R., Allinger, N. L., Clark, T., Gasteiger, J., Kollman, P. A., Schaefer, H. F., III, Eds.; John Wiley & Sons: Chichester, U.K., 1998; Vol. 5, pp 3094−3104. (d) Truhlar, D. G.; Garrett, B. C.; Klippenstein, S. J. *J. Phys. Chem.* **1996**, *100*, 12771.
(2) (a) Viggiano, A. A.; Paschkewich, J.; Morris, R. A.; Paulson, J. F.; González-Lafont, A.; Truhlar, D. G. *J. Am. Chem. Soc.* **1991**, *113*, 9404. (b) Liu, Y.-P.; Lynch, G. C.; Truong, T. N.; Lu, D.-h.; Truhlar, D. G.; Garrett, B. C. *J. Am. Chem. Soc.* **1993**, *115*, 2408. (c) Villà, J.; Corchado, J. C.; González-Lafont, A.; Lluch, J. M.; Truhlar, D. G. *J. Am. Chem. Soc.* **1998**, *120*, 12141. (d) Pu, J.; Corchado, J. C.; Truhlar, D. G. *J. Chem. Phys.* **2001**, *115*, 6266. (e) Pu, J.; Truhlar, D. G. *J. Chem. Phys.* **2002**, *117*, 1479.
(3) Singleton, D. A.; Hang, C.; Szymanski, M. J.; Greenwald, E. E. *J. Am. Chem. Soc.* **2003**, *125*, 1176.
(4) Singleton, D. A.; Hang, C.; Szymanski, M. J.; Mayer, M. P.; Leach, A. G.; Kuwata, K. T.; Chen, J. S.; Greer, A.; Foote, C. S.; Houk, K. N. *J. Am. Chem. Soc.* **2003**, *125*, 1319.
(5) Reyes, M. B.; Lobkovsky, E. B.; Carpenter, B. K. *J. Am. Chem. Soc.* **2002**, *124*, 641.
(6) Bakken, V.; Danovich, D.; Shaik, S.; Schlegel, H. B. *J. Am. Chem. Soc.* **2001**, *123*, 130.
(7) Valtazanos, P.; Ruedenberg, K. *Theor. Chim. Acta* **1986**, *69*, 281.
(8) Krauss, W. A.; Depristo, A. E. *Theor. Chim. Acta* **1986**, *69*, 309.
(9) Basilevsky, M. V. *Theor. Chim. Acta* **1987**, *72*, 63.
(10) Baker, J.; Gill, P. M. W. *J. Comput. Chem.* **1988**, *9*, 465.
(11) Bosch, E.; Moreno, M.; Lluch, J. M.; Bertrán, J. *Chem. Phys. Lett.* **1989**, *160*, 543.
(12) Taketsugu, T.; Hirao, K. *J. Chem. Phys.* **1993**, *99*, 9806.
(13) Taketsugu, T.; Hirao, K. *J. Mol. Struct. (THEOCHEM)* **1994**, *310*, 169.
(14) Taketsugu, T.; Tajima, N.; Hirao, K. *J. Chem. Phys.* **1996**, *105*, 1933.
(15) Simons, J. *Int. J. Quantum Chem.* **1993**, *48*, 211.
(16) Simons, J. *Int. J. Quantum Chem.* **1993**, *48*, 309.
(17) Hirsch, M.; Quapp, W.; Heidrich, D. *Phys. Chem. Chem. Phys.* **1999**, *1*, 5291.
(18) Ramquet, M.-N.; Dive, G.; Dehareng, D. *J. Chem. Phys.* **2000**, *112*, 4923.
(19) Lasorne, B.; Dive, G.; Lauvergnat, D.; Desouter-Lecomte, M. *J. Chem. Phys.* **2003**, *118*, 5831.

singlet ($^1\Delta_g$) oxygen ($^1O_2$) with tetramethylethylene affecting the product ratios. In effect, a significant KIE was experimentally[20] observed on the product distribution (**2** versus **3**) in the addition of $^1O_2$ to the stereoisomerically d_6-labeled tetramethylethylene **1**. In the final products, one oxygen atom becomes bonded to one of the carbon atoms supporting the double bond in **1**, while the other oxygen atom abstracts either a hydrogen or a deuterium atom from a $-CH_3$ or a $-CD_3$ group, respectively, attached to the other carbon atom of the double bond, leading to **2** or **3**, with rate constants k_H or k_D. k_H/k_D turns out to be 1.4. Very recently, CCSD(T)/6-31G* single-point energy calculations on a grid of B3LYP/6-31G* geometries were carried out by Singleton et al.[3,4] showing that the MEP for the perprotio reaction involves two adjacent saddle points without an intervening intermediate. The first one is a relatively early C_s-symmetric rate-limiting transition-state structure (**TS1**) for the attack of $^1O_2$ to the ethylene. At this saddle point, the hydrogen abstraction has not yet started. The second one (**TS2**), also C_s-symmetric, is a perepoxide-like structure. **TS2** is actually a transition-state structure that corresponds to the interconversion of the two products **2** and **3**. The MEP connects **TS1** and **TS2** but becomes unstable in-between, when the **VRI** is reached. At the **VRI**, the frequency corresponding to a generalized normal mode orthogonal to the MEP goes to zero, marking the place where a valley turns into a ridge, indicating possible branching of the PES. Since **TS1** is previous to the branching, and **TS2** has no enthalpic or entropic barrier for its decomposition, Singleton et al.[4] claim that selectivity in the area of the **VRI** cannot be analyzed using transition-state theory. Instead, in an accompanying paper, Singleton et al.[3] have performed quasiclassical direct dynamics calculations on the B3LYP/6-31G* PES of **1**. The trajectories were started in a region between **TS1** and the **VRI**, centered on the MEP with both O−C distances of 1.95 Å. The trajectories were initialized in two ways: at 0 K, giving each mode in total only its zero-point energy with a random sign for its initial velocity, or at 263 K, using a Boltzmann sampling of vibrational levels along with a Boltzmann sampling of translational energy for the C_s-symmetric approach of the O_2 toward the olefinic carbons. Out of 183 runs at 0 K, with 95% confidence, the simulation's nominal k_H/k_D of 2.1 was between 1.3 and 3.4. The selectivity was lower for the higher temperature 263 K simulation after 257 runs, which gave a nominal k_H/k_D of 1.38 with a standard deviation of 0.17. From those results, the authors have concluded that this selectivity is a new form of KIE, dynamical in origin, unrelated to the usual effect of zero-point energies on barriers.

The purpose of the present work is to show that, using variational transition state theory in a convenient way, distinct dynamical bottlenecks leading to each particular product can be located in a reaction including a VRI with no additional dynamic calculations being required to predict successfully the experimental product distributions. To this aim, as a challenging example, we have applied VTST to determine the intramolecular KIEs affecting product branching in the reaction of singlet oxygen with d_6-tetramethyethylene **1** and with the corresponding tritiated derivative.

Details of the Electronic Structure Calculations. For the sake of comparison between the VTST results of this paper and the quasiclassical simulation by Singleton et al.,[3] we have just used their own electronic level of calculation.The PES obtained by Singleton et al.[4] by means of CCSD(T)/ 6-31G* single-point energy calculations on a grid of B3LYP/6-31G* is qualitatively shown in Figure 1. In this figure, we have marked the relevant points mentioned in the Introduction. Anyway, the quasiclassical direct dynamics calculations by Singleton et al.[3] have been carried out on a B3LYP/6-31G* PES. Then, the VTST calculations in this paper also correspond to that B3LYP/6-31G* PES. This PES overestimates the energy of $^1O_2$ but closely models the CCSD(T)/6-31G* PES as the $^1O_2$ draws close (O_1-C_1 or $O_1-C_2 < 2.3$ Å) to the ethylene.[3,4] Unfortunately, **TS1** is an early transition state structure in the CCSD(T)/6-31G*//B3LYP/6-31G* PES ($O_1C_1 = O_1C_2 = 2.38$ Å) but does not exist as an actual saddle point in the B3LYP/6-31G* PES because of the bad description of the isolated $^1O_2$. In this paper, we will refer to the **TS1** in the B3LYP/6-31G* PES as a structure with a geometry corresponding to the CCSD(T)/6-31G*//B3LYP/6-31G* **TS1** and an energy calculated at the B3LYP/6-31G* level at that geometry. As a matter of fact, this **TS1** would be needed to calculate the global rate constant of the reaction, but, as shown below, it is not explicitly required to determine the branching ratio of the products.

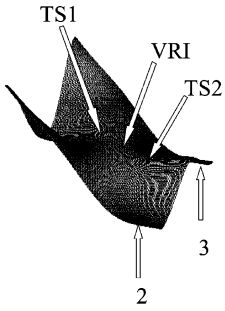

Figure 1. Qualitative potential energy surface.

To locate the B3LYP/6-31G* **VRI** point, we have analyzed the vibrational frequencies of the normal modes perpendicular to the MEP. For this purpose, the Page−McIver algorithm[21] has been used to compute the MEP from **TS1** and by stepping down in the direction of the gradient with a step size of $\delta s = 0.015$ au (where s denotes the distance along the MEP in an isoinertial mass-scaled Cartesian coordinate system with a scaling mass equal to 1 amu). As expected, the MEP preserves the C_s symmetry. The step size has been reduced to $\delta s = 0.0075$ au from a structure with O_1-C_1 and O_1-C_2 distances of 1.95 Å. In this region of the MEP, the force constant matrix in mass-scaled Cartesian coordinates has been evaluated at each step and a projector has been used to project the direction along the reaction path as well as overall rotations and translations out of the space associated with the nonzero eigenvalues.[22] The diagonalization of the projected force constant matrix showed that the lowest harmonic vibrational frequency corresponding to a normal mode perpendicular to the MEP goes to nearly zero (its actual value is of 5i cm^{-1}) at a structure with the O_1-C_1 and O_1-C_2 distances equal to 1.902 Å. This point can be identified as the **VRI**, where the valley relative to that orthogonal mode becomes a ridge. This **VRI** structure lies 2.81 kcal/mol below **TS1** and only 1.0 kcal/mol above the **TS2** structure (O_1-

(20) (a) Grdina, B.; Orfanopoulos, M.; Stephenson, L. M. *J. Am. Chem. Soc.* **1979**, *101*, 3112. (b) Orfanopoulos, M.; Smonou, I.; Foote, C. S. *J. Am. Chem. Soc.* **1990**, *112*, 3607.

(21) Page, M.; McIver, J. W., Jr. *J. Chem. Phys.* **1988**, *88*, 922.
(22) Miller, W. H.; Handy, N. C.; Adams, J. E. *J. Chem. Phys.* **1980**, *72*, 99.

$C_1 = O_1-C_2 = 1.67$ Å). Following the gradient, the MEP remains on the ridge of the PES until the system reaches the saddle point structure **TS2** where the direction associated with the orthogonal imaginary frequency normal mode corresponds to the conversion of the two final products (**2** and **3**) into each other. All these calculations of the PES for the $^1O_2$ + d_6-tetramethylethylene reaction were carried out with GAUSSRATE9.0 package,[23] which is an interface linking POLYRATE9.0[24] and GAUSSIAN98.[25]

Results and Discussion

In this section, we will present the main results of the paper along with a discussion of the dynamical methods we have used.

From the **VRI** geometry on the MEP, the two reaction paths leading to the isotope-labeled products (**2** and **3**) were initiated by stepping down in the direction of the normalized imaginary frequency eigenvector which is associated with the breaking of the C_s-symmetry of the MEP. At this point, a small modification of the GAUSSRATE9.0 code was necessary to force the system to follow the two bifurcating reaction paths. Concretely, to define the initial step at the **VRI** on the direction of those two bifurcating reaction paths, we only needed to substitute in the code of normalized gradient vector at the **VRI** by the above-mentioned normalized eigenvector associated with the breaking of the C_s-symmetry.

After the initial step, the Page−McIver algorithm was used again with a gradient step size of $\delta s = 0.05$ au to describe the bifurcating reaction paths all the way down to the final products. At every gradient step size, the projected force constant matrix was also computed. The generalized vibrational frequencies and the generalized normal modes orthogonal to the reaction path were obtained by diagonalization of those projected force constant matrixes using again mass-scaled Cartesian coordinates within the harmonic approximation. From those frequencies, the harmonic zero-point energy correction at each step along the path can be calculated. The interpolated variational transition state theory by mapping (IVTST-M)[26] was then used to interpolate the information along the bifurcating reaction paths to obtain the adiabatic ground-state potential energy curve at each side of the **VRI** as a function of s (the adiabatic energy includes classical potential energy and zero-point energy contributions). Neither the H-abstraction path leading to **2** nor the D-abstraction path leading to **3** present an adiabatic potential energy barrier.

Accordingly to VTST, we define a sequence of generalized transition states corresponding to the reaction coordinate as dividing surfaces which are orthogonal to the reaction path intersecting it at a particular value of s. The partition functions at reactants and at the generalized transition states are evaluated as products of the electronic, vibrational, and rotational partition functions and for bimolecular reactions, as in this case, a relative translational partition function per unit volume. For the electronic and vibrational partition functions, we use quantum expressions including only the ground-state electronic contribution whereas the translational and rotational partition functions are evaluated classically. The vibrational partition function is obtained as a product of the contributions corresponding to each individual normal mode. In absence of tunneling, the generalized rate constant corresponding to the dividing surface intersecting at s is defined as

$$k^{GT}(T, s) = \sigma \frac{k_B T}{h} \frac{Q^{GT}(T, s)}{Q^R(T)} \exp\left(-\frac{V(s)}{k_B T}\right) \qquad (1)$$

where T is the temperature, σ is the symmetry factor, k_B is Boltzmann's constant, h is Planck's constant, $V(s)$ is the classical potential energy at s with zero of energy at the overall classical energy of reactants, $Q^R(T)$ is the reactant partition function per unit volume again with zero of energy at reactants, and $Q^{GT}(T,s)$ is the generalized transition-state partition function with zero of energy at $V(s)$ and excluding the reaction coordinate. For all the partition functions, the rotational symmetry numbers are removed, as they are included in σ. The location of the canonical variational transition state (CVT) is then determined by

$$k^{CVT}(T) = \min_s k^{GT}(T, s) = k^{GT}(T, s^{CVT}(T)) \qquad (2)$$

which is equivalent to maximize with respect to s the generalized free energy of activation defined as

$$\Delta G^{GT,o}(T, s) = RT\left[\frac{V(s)}{k_B T} - \ln \frac{Q^{GT}(T, s)}{Q^R(T)\, K^o}\right] \qquad (3)$$

where $K°$ is the reaction quotient evaluated at the standard state, the free energy is calculated in kcal/mol, and the standard state, as usual in VTST, is 1 molecule cm^{-3}.

The first step from the **VRI** along the eigenvector associated with the imaginary frequency (orthogonal to the MEP) leads to a point very close to the **VRI**. At that point, once the C_s-symmetry has been already broken, the gradient is almost parallel to the gradient at the **VRI** (the angle between them is just 0.55°). In other words, after the first orthogonal step to the MEP, both bifurcating reaction paths are initially almost parallel to the **TS1** to **TS2** MEP, although they progressively diverge from it as the reaction progresses toward the respective final products (**2** or **3**). Then, during a range of values of s (about 1.9 au) from the **VRI** geometry, one of the frequencies is imaginary (its associated eigenvector still has an important component orthogonal to the original ridge) along each bifurcating path. In this region of the bifurcating path, the harmonic oscillator treatment cannot be used to calculate the vibrational partition function of the corresponding normal mode.

Normally, when the reaction path lies along the bottom of a valley, each one-dimensional potential energy profile orthogonal

(23) Corchado, J. C.; Chuang, Y.-Y.; Coitiño, E. L.; Truhlar, D. G. *Gaussrate 9.0*; University of Minnesota: Minneapolis, MN, 2002 (http://comp.chem.umn.edu/polyrate).
(24) Corchado, J. C.; Chuang, Y.-Y.; Fast, P. L.; Villà, J.; Hu, W.-P.; Liu, Y.-P.; Lynch, G. C.; Nguyen, K. A.; Jackels, C. F.; Melissas, V. S.; Lynch, B. J.; Rossi, I.; Coitiño, E. L.; Fernandez Ramos, A.; Pu, J.; Albu, T. V.; Steckler, R.; Garrett, B. C.; Isaacson, A. D.; Truhlar, D. G. *POLYRATE 9.0*; University of Minnesota: Minneapolis, MN, 2002.
(25) Frisch, M. J.; Trucks, G. W.; Schlegel, H. B.; Scuseria, G. E.; Robb, M. A.; Cheeseman, J. R.; Zakrzewski, V. G.; Montgomery, J. A., Jr.; Stratmann, R. E.; Burant, J. C.; Dapprich, S.; Millam, J. M.; Daniels, A. D.; Kudin, K. N.; Strain, M. C.; Farkas, O.; Tomasi, J.; Barone, V.; Cossi, M.; Cammi, R.; Mennucci, B.; Pomelli, C.; Adamo, C.; Clifford, S.; Ochterski, J.; Petersson, G. A.; Ayala, P. Y.; Cui, Q.; Morokuma, K.; Malick, D. K.; Rabuck, A. D.; Raghavachari, K.; Foresman, J. B.; Cioslowski, J.; Ortiz, J. V.; Baboul, A. G.; Stefanov, B. B.; Liu, G.; Liashenko, A.; Piskorz, P.; Komaromi, I.; Gomperts, R.; Martin, R. L.; Fox, D. J.; Keith, T.; Al-Laham, M. A.; Peng, C. Y.; Nanayakkara, A.; Gonzalez, C.; Challacombe, M.; Gill, P. M. W.; Johnson, B. G.; Chen, W.; Wong, M. W.; Andres, J. L.; Head-Gordon, M.; Replogle, E. S.; Pople, J. A. *Gaussian 98*, Revision A.6 and A.7; Gaussian, Inc.: Pittsburgh, PA, 1998.
(26) Corchado, J. C.; Coitiño, E. L.; Chuang, Y.-Y.; Fast, P.; Truhlar, D. G. *J. Phys. Chem. A* **1998**, *102*, 2424.

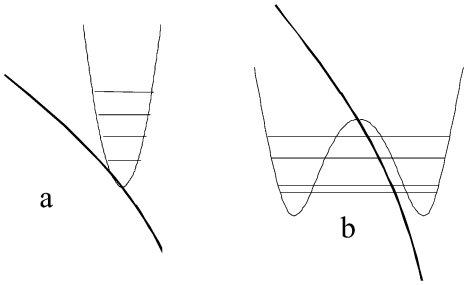

Figure 2. One-dimensional potential energy profile orthogonal to the path, when the reaction path (thick line) lies along the bottom of a valley (a) or along a ridge (b).

to the path at s can be considered to be parabolic (see Figure 2a), its classical potential energy minimum being located at the reaction path (with a potential energy equal to $V(s)$) in such a way that the harmonic treatment is applied (although some anharmonicity corrections can be used in some cases). Indeed, each vibrational energy level contributes with a positive energy (recall that the origin of energies is $V(s)$) to the exponents E_i which appear in the sum which defines the vibrational partition function of the corresponding normal mode:

$$q = \sum_i e^{-(E_i/k_B T)} \tag{4}$$

Then, q turns out to be smaller than 1, diminishing the value of $Q^{GT}(T, s)$ and giving a positive contribution to the generalized activation free energy in eq 3.

The scenario is very different when the reaction path is in a ridge.[27] We will focus now on our two bifurcating reaction paths. As mentioned above, they are built following the gradient. So, along the directions orthogonal to the path, the first derivative is zero. The projected force constant matrix provides the generalized vibrational frequencies and the generalized normal modes orthogonal to the reaction path. If one of those frequencies is imaginary, the reaction path is in a ridge. Then, the one-dimensional potential energy profile at s along the corresponding generalized normal mode is rather a double well (see Figure 2b), with its classical potential energy maximum being located at the reaction path. Even in absence of symmetry, this is so because along this direction the first and second derivatives are, respectively, zero and negative. In this case, the corresponding vibrational energy levels, if needed, could be found by solving in some way the nuclear Schrödinger equation associated with that one-dimensional potential energy profile.[27a] Indeed, those vibrational levels contribute with a negative energy to the exponents E_i in eq 4, so leading to a big value ($\gg 1$) of the vibrational partition function q of the normal mode and, as a consequence, giving an important negative contribution to the generalized activation free energy in eq 3. The effect grows with the depth of the two lateral wells. This is what occurs along an arc length of about 1.9 au from the **VRI** for the two bifurcating paths. This region will include a generalized activation free-energy minimum. The dynamical bottleneck associated with a generalized activation free-energy maximum appears beyond that region, when each bifurcating reaction path has reached its corresponding valley.

(27) (a) Garrett, B. C.; Truhlar, D. G.; Wagner, A. F.; Dunning, T. H., Jr. *J. Chem. Phys.* **1983**, *78*, 4400. (b) Miller, W. H. *J. Phys. Chem.* **1983**, *87*, 3811.

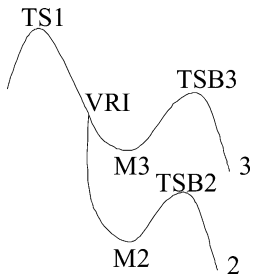

Figure 3. Schematic diagram showing the generalized activation free energy as a function of s.

At this point, the picture of the overall reaction can be described as follows in terms of the generalized free energy of activation as a function of s (see the schematic diagram shown in Figure 3). A first dynamical bottleneck exists (a maximum of $\Delta G^{GT,o}$) near the rate-limiting transition-state structure **TS1** on the MEP. Once on each bifurcating reaction path, after the **VRI**, a quite deep minimum of $\Delta G^{GT,o}$ (**M2** or **M3**, respectively) appears, followed by the corresponding second dynamical bottleneck (a second maximum of $\Delta G^{GT,o}$, **TSB2** or **TSB3**, respectively). At last, the final product (**2** or **3**, respectively) is formed.

Since there are several bottlenecks and two competitive bifurcating reaction paths, we have used a generalization of the competitive canonical unified statistical (CCUS) model. Let k_{TS1}, k_{TSB2}, and k_{TSB3} be the rate constants corresponding to the **TS1**, **TSB2**, and **TSB3** bottlenecks, respectively. Let k_{M2} and k_{M3} be the one-way flux rate constants evaluated at the dividing surfaces **M2** and **M3**, respectively. Then, the expression of the overall CCUS[28] rate constant k^{CCUS} is obtained by straightforward application of the well-known procedures for combining fluxes in parallel and series, which yields

$$\frac{1}{k^{CCUS}} = \frac{1}{k_{TS1}} + \frac{1}{k'_2 + k'_3} \tag{5}$$

with

$$\frac{1}{k'_2} = -\frac{1}{k_{M2}} + \frac{1}{k_{TSB2}} \tag{6}$$

$$\frac{1}{k'_3} = -\frac{1}{k_{M3}} + \frac{1}{k_{TSB3}} \tag{7}$$

The individual rate constants leading to products **2** and **3**, respectively, are given by

$$k_2 = k^{CCUS} \frac{k'_2}{k'_2 + k'_3} \tag{8}$$

$$k_3 = k^{CCUS} \frac{k'_3}{k'_2 + k'_3} \tag{9}$$

According to the CUS theory,[29−31] all the rate constants are calculated with respect to the same reactants. Therefore, $Q^R(T)$ is the same in all cases. As stated in the Introduction, the aim of this paper is to show that VTST is able to determine the branching ratio (in the present case, the KIE) of the products even taking into account the existence of a VRI. On the other

(28) Hu, W.-P.; Truhlar, D. G. *J. Am. Chem. Soc.* **1996**, *118*, 860.
(29) Miller, W. H. *J. Chem. Phys.* **1976**, *65*, 2216.
(30) Garrett, B. C.; Truhlar, D. G. *J. Chem. Phys.* **1982**, *76*, 1853.
(31) Hu, W.-P.; Truhlar, D. G. *J. Am. Chem. Soc.* **1995**, *117*, 10726.

Table 1. Canonical Variational Transition State Free-Energy Barriers (in kcal/mol) for the H- and D-Abstraction Bifurcating Reaction Paths, Difference between Them, and Intramolecular Kinetic Isotope Effects as a Function of Temperature (in K)[a]

T	$\Delta G_H^{CVT,o}$	$\Delta G_D^{CVT,o}$	$\Delta\Delta G^{CVT,o}_{D-H}$	k_H/k_D
150	4.777	4.833	0.056	1.207
200	11.372	11.431	0.059	1.160
263	19.698	19.760	0.062	1.126
300	24.586	24.649	0.063	1.111
400	37.765	37.831	0.066	1.087
500	50.888	50.955	0.067	1.070

[a] The standard state is 1 molecule cm^{-3}.

hand, the **VRI** structure lies 35.68 kcal/mol above the final products **2** and **3** in terms of classical potential energy. This indicates that the fall in energy from the ridge is huge, leading to a very deep minima of $\Delta G^{GT,o}$ and to very high fluxes at **M2** and **M3**. Then, as usual in CUS calculations,[28−31] the terms $(1/k_{M2})$ and $(1/k_{M3})$ in eqs 6 and 7 can be neglected, in such a way that, finally, the branching ratio (i.e., the KIE in this case) is given by

$$\frac{k_2}{k_3} = \frac{k_{TSB2}}{k_{TSB3}} \tag{10}$$

In other words, here the KIE can be calculated from the ratio between the two rate constants corresponding to the dynamical bottlenecks that appear in each bifurcating reaction path. This fact avoids in this case the explicit calculation of the double-well vibrational levels corresponding to the zone of the ridge.

In Table 1, the canonical variational transition state free-energy barriers ($\Delta G^{CVT,o}(T) = \Delta G^{GT,o}(T, s^{CVT}(T))$ with respect to the separated reactants are given as a function of temperature for the H-abstraction and the D-abstraction bifurcating reaction paths.

From the figures in Table 1, it can be observed that by using VTST, two distinct dynamical bottlenecks leading to each particular product (**2** or **3**) can be located at any temperature. Let us analyze, for instance, the bottleneks at 150 K. At this temperature, **TSB2** and **TSB3** appear at *s* values of 2.826 au and 2.674 au, respectively, measured from the **VRI** along each bifurcating reaction path. In terms of classical potential energy, **TSB2** and **TSB3** at 150 K are 3.871 and 3.884 kcal/mol below **TS1**. The geometries of the corresponding points of the bifurcating paths are shown in Figure 4. Both structures are clearly away from the C_s-symmetry preserved along the **TS1** to **TS2** MEP. In the structure associated with **TSB2**, which will lead to the final product **2**, the O_1 atom is clearly closer to the C_2 atom than to the C_1 atom, while the O_2 atom is already approaching a hydrogen atom of a $-CH_3$ group. Conversely, in the structure associated with **TSB3**, which will lead to the final product **3**, the O_1 atom is clearly closer to the C_1 atom than to the C_2 atom, while the O_2 atom is already initiating the abstraction of a deuterium atom of a $-CD_3$ group.

A normal (bigger than 1) KIE is obtained at all the studied temperatures. The free-energy differences at each temperature between the H-abstraction and the D-abstraction bottlenecks (shown in the fourth column of Table 1) are mainly due to the zero-point energy differences of the two canonical variational transition states. For instance, the free-energy difference between the two free-energy maxima at 150 K is 0.056 kcal/mol and the corresponding adiabatic potential energy difference is 0.065

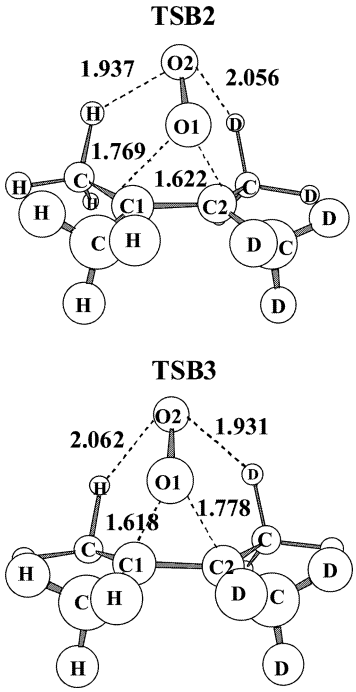

Figure 4. Geometries of the structures corresponding to the dynamical bottlenecks **TSB2** and **TSB3**. Distances are given in Å.

kcal/mol. The main reasons for this difference are the C−H generalized normal mode of lowest frequency and the C−D generalized normal mode of lowest frequency (see the evolution of frequencies along the bifurcating reaction paths in Table S1). As expected, they correspond to the hydrogen and the deuterium atoms, respectively, closest to the O_2 atom (see Figure 4). It can also be observed that the free-energy difference between the H-abstraction and D-abstraction free-energy barriers slightly increases as temperature goes up because the canonical variational transition states slightly move toward products where the adiabatic potential energy difference takes a value of 0.15 kcal/mol. In contrast, the KIE decreases as temperature increases because the change in the free-energy differences between H- and D-bottlenecks is rather small compared to the change of temperature. The most important fact here is that these normal KIEs, calculated by using VTST, show the practical capability of this theory for discerning between the two branching reaction paths of the $^1O_2$ + d_6-tetramethylethylene chemical process. The difference with the experimental value of 1.4 at 263 K can be attributed to the fact that the B3LYP/6-31G* PES (used in this paper to compare with the quasiclassical direct dynamics calculations by Singleton at al.[3]) is not accurate enough (in terms of potential energies and frequencies) to provide quantitative results.

In addition, even though to our knowledge there are no experimental results for the reaction of $^1O_2$ with the tritiated derivative of tetramethylethylene (i.e., the six deuterium atoms in reactant **1** having been substituted by 6 tritium atoms), we have analogously repeated all the calculations for the heavier isotope. The results are presented in Table 2. As expected, the normal KIES (k_H/k_T) are bigger than the corresponding k_H/k_D values. However, the trends with temperature of the different magnitudes presented in Table 2 are similar to the ones observed for the deuterated reaction.

At this point, the reason of why the bifurcating reaction paths start at the **VRI** has to be discussed. VTST requires to build up

Table 2. Canonical Variational Transition State Free-Energy Barriers (in kcal/mol) for the H- and T-Abstraction Bifurcating Reaction Paths, Difference between Them, and Intramolecular Kinetic Isotope Effects as a Function of Temperature (in K)[a]

T	$\Delta G_H^{CVT,0}$	$\Delta G_T^{CVT,0}$	$\Delta\Delta G^{CVT,0}{}_{T-H}$	k_H/k_T
150	4.844	4.915	0.071	1.269
200	11.444	11.520	0.076	1.211
263	19.772	19.854	0.082	1.170
300	24.660	24.745	0.085	1.153
400	37.839	37.931	0.092	1.123
500	50.960	51.058	0.098	1.104

[a] The standard state is 1 molecule cm^{-3}.

a continuous set of trial nonintersecting dividing surfaces separating reactants and products along the reaction path. In practice, just a discrete subset of them, built up as hyperplanes orthogonal to the reaction path (unless the RODS method[32,33] is applied), is used for the calculations. According to that, it is not possible to construct a set of suitable dividing surfaces from **TS1** to **TS2** along the MEP and then from **TS2** to **2** and **3** for several reasons. The dividing surfaces along the MEP would be orthogonal to it, whereas the dividing surface at **TS2** would be orthogonal to the transition vector at this saddle point. As a consequence, the dividing surface at **TS2** would be orthogonal to the precedent dividing surfaces along the **TS1** to **TS2** MEP. This would produce un unrealistic sudden discontinuity in the results of the calculations, and indeed the hyperplane dividing surface at **TS2** would intersect the precedent ones. In addition, the dividing surfaces at **TS2** and along the **TS2** to **2** (or **3**) MEP do not separate the reactants from products, but **2** from **3** (that is, as stated above, **TS2** is a transition-state structure corresponding just to the interconversion of the final products **2** and **3**). Then, we agree with Singleton at al.[3,4] if what they are stating is that VTST cannot be applied in this reaction using a reaction path passing through **TS2**. The novelty of the present paper is that we show that VTST can be applied along a suitable reaction path which bifurcates before **TS2**, leading to reasonable KIEs in comparison with the quasiclassical direct dynamics simulations by Singleton et al.[3] and with the experimental results (although we have used the B3LYP/6-31G* for a better comparison with the dynamics simulation).

The problems concerning **TS2** diminish as the starting point of the bifurcating reaction path approaches the **VRI**. In addition, VTST assumes that not only the electronic degrees of freedom adjust adiabatically to motion along the reaction path (this is the Born−Oppenheimer approximation) but also all other nuclear degrees of freedom adjust adiabatically, that is, preserve their quantum numbers. However, sharp changes in the direction of the reaction path cause large curvature couplings between the various degrees of freedom, inducing a nonadiabatic behavior.[1a,27b] It is better to choose a smooth reaction path to minimize the coupling. In this sense, the reaction path is disturbed when the bifurcating paths start from the MEP, but the change is smoother near the **VRI** (recall the small angle mentioned above). Thus, it seems that the best choice is to start the bifurcating reaction path at the **VRI** or just after it.

(32) González-Lafont, A.; Villà, J.; Lluch, J. M.; Bertrán, J.; Steckler, R.; Truhlar, D. G. *J. Phys. Chem. A* **1998**, *102*, 3420.
(33) Villà, J.; Truhlar, D. G. *Theor. Chem. Acc.* **1997**, *97*, 317.

Concluding Remarks

From the results obtained in this paper, we can conclude that, provided that a suitable reaction path is chosen, variational transition state theory is a realistic tool to calculate the branching ratio of products (i.e., the intramolecular KIE) in the reaction of singlet oxygen with d_6-tetramethyethylene **1** and with the corresponding tritiated derivative, despite the existence of a valley-ridge inflection point in the minimum-energy path after the rate-limiting transition state of the global reaction. Although additional theoretical work is needed to extend the present conclusion to other analogous reacting systems, we think that the strategy proposed here can be very useful to study other reactions with bifurcating reaction paths. So, it seems that the existence of a valley-ridge inflection point does not involve a nonstatistical dynamics behavior which would imply that statistical theories for reaction rates are inadequate. This fact would make it possible that effects of experimental interest (temperature, substituents, isotopic mass, etc.) could be easily understood and predicted in terms of kinetic magnitudes (free-energy barriers and their components), so avoiding the expensive generation of the huge number of dynamical trajectories required to obtain statistically significant results. In this sense, for the particular case treated here, the experimental isotopic selectivity turns out to be mainly due to the slight (but significant enough) difference of zero-point energy between both bifurcating reaction paths.

Acknowledgment. We are grateful for financial support from the Spanish "Ministerio de Ciencia y Tecnología" and the "Fondo Europeo de Desarrollo Regional" through project No. BQU2002-00301.

Supporting Information Available: Classical and adiabatic potential energies, frequencies, and more relevant geometrical parameters along the bifurcating reaction paths. This material is available free of charge via the Internet at http://pubs.acs.org.

JA039561R